Shock formation in an exclusion process with creation and annihilation

M. R. Evans,[1] R. Juhász,[2] and L. Santen[2]
[1]*School of Physics, University of Edinburgh, Mayfield Road, Edinburgh EH9 3JZ, United Kingdom*
[2]*Theoretische Physik, Universität des Saarlandes, 66041 Saarbrücken, Germany*
(Received 26 March 2003; published 19 August 2003)

We investigate shock formation in an asymmetric exclusion process with creation and annihilation of particles in the bulk. We show how the continuum mean-field equations can be studied analytically and hence derive the phase diagrams of the model. In the large system-size limit direct simulations of the model show that the stationary state is correctly described by the mean-field equations, thus the predicted mean-field phase diagrams are expected to be exact. The emergence of shocks and the structure of the phase diagram are discussed. We also analyze the fluctuations of the shock position by using a phenomenological random walk picture of the shock dynamics. The stationary distribution of shock positions is calculated, by virtue of which the numerically determined finite-size scaling behavior of the shock width is explained.

DOI: 10.1103/PhysRevE.68.026117 PACS number(s): 05.60.−k, 87.16.Uv, 87.16.Nn, 05.70.Ln

I. INTRODUCTION

The analysis of self-driven particle models is a central issue of nonequilibrium statistical mechanics [1–5]. These models show a variety of generic nonequilibrium effects, in particular, in low dimensions. Although the behavior is generally rather complex, some models are simple enough to be analyzed in great detail. In rare cases, it is even possible to obtain exact results for the stationary state [2,5]. A very prominent example of such a model is the asymmetric exclusion process (ASEP) which comprises particles hopping in a preferred direction under the constraint that they cannot occupy the same lattice site. Exact solutions for the stationary state exist for periodic [1,6] and open boundary conditions [7,8] and different update schemes [9–11]. Therefore, this model has been used in order to develop more general concepts for systems far from equilibrium, e.g., a free-energy formalism [12]. Variants of the model have also allowed the study of shocks which are discontinuities in the density of particles over a microscopic distance [13].

The ASEP and related models are not only of academic interest, but have a number of important applications, e.g., as simplified traffic models [4]. Here, we are interested in a variant of the ASEP, which is motivated by biological transport processes in living cell systems, where particle nonconservation in the bulk of the system is allowed [14] (see also Ref. [28]).

An important feature of living cells is their ability to move and to generate forces [15–17]. On a microscopic level these forces are mostly generated by motor proteins [18,19], which are able to perform directed motion along one-dimensional paths or filaments.

Many different motor proteins can be distinguished [18], but they have a few common properties: a head, which can couple to a filament, where it performs a directed stochastic motion and a tail, which is attached to a specific load, which has to be transported through the cell. The coupling of the motor protein heads to the filament is reversible, thus the motor proteins will attach to the filament, perform stochastic directed motion for some time, and eventually detach from the filament. The typical distance between attachment and detachment of the motor protein to the filament depends on the particular type of filament.

To a first approximation, the motion of many motor proteins along a filament can be modeled by the asymmetric exclusion process. An important feature, which is not described by the ASEP, is the attachment and detachment of the motor-protein heads. This feature has been included in a recent model by Parmeggiani *et al.* [14] (see also Ref. [28]), which can be viewed as a grand-canonical counterpart of the ASEP in the sense that in the bulk the particle number is not conserved.

For open boundary conditions, however, the situation is different. In this case, if the rates of attachment scale correctly with system length, one observes a subtle interplay between the left, right, and bulk particle reservoirs. If we fix the attachment and detachment rates then there are whole regions of the phase diagram (spanned by the densities of the boundary reservoirs) where one observes the *localization* of shocks in the bulk of the system. This is in contrast to the ASEP, where shocks move with constant velocity and are generally driven to the boundary of an open system. The shock has zero velocity only on the phase boundary where two phases of different density coexist. Even in this case, the shock is not localized since it diffusively explores the whole system.

The physical origin of the shock localization in the present model and a discussion of the phase diagram, in particular, the phase where shocks appear are the subject of this paper. We shall show how the phase diagram can be predicted through simple considerations pertaining to a continuum mean-field description that only retains first-order terms, i.e., the phase diagram can be predicted through the study of a simple first-order nonlinear partial differential equation. Going beyond the mean level, in the shock phase we describe the dynamics of the shock by a random walker with space-dependent hopping rates. In this way, the localization of the shock can be understood.

The paper is organized as follows. In the following section, we give the definition of the model and introduce the stationary solution in case of periodic boundary conditions. In Sec. III, we introduce the mean-field equations for the

open system and discuss their solution by means of characteristics. Then we discuss the stationary solutions on the mean-field level and compare the mean-field results to Monte Carlo (MC) simulations. Fluctuations of the shock positions are analyzed in Sec. V and finally, some concluding remarks are given in the last section.

II. MODEL

We consider a one-dimensional open chain of N sites, which can either be empty ($\tau_i=0$) or be occupied with one particle ($\tau_i=1$). Particles can jump to the neighboring site if it is empty. In addition, the bulk sites are coupled to particle reservoirs, i.e., particles are attached with rate ω_A and deleted with rate ω_D. The particle reservoirs at the boundaries are different from the bulk. At the first site, particles are attached with rate α and deleted with rate ω_D, while at the last site particles attach with rate ω_A and are deleted with rate β [14]. By a rate r it is meant that in infinitesimal time interval dt, the probability of the event occurring is rdt. Schematically, the dynamics can be written as follows:

$$* 0 \overset{\omega_A}{\longrightarrow} * 1, \tag{1}$$

$$1 * \overset{\omega_D}{\longrightarrow} 0 *, \tag{2}$$

$$1\ 0 \overset{1}{\longrightarrow} 0\ 1, \tag{3}$$

where $1(0)$ corresponds to an empty (occupied) site and * implies that the update is independent of the state.

The dynamics at the left-hand boundary (site 1) is insertion of particles

$$0 \overset{\alpha}{\longrightarrow} 1, \tag{4}$$

and at the right-hand boundary (site N) is removal of particles

$$1 \overset{\beta}{\longrightarrow} 0. \tag{5}$$

The exact equation for the evolution of the particle densities $\langle \tau_i \rangle$ away from the boundaries ($1<i<N$) is given by

$$\frac{d\langle \tau_i \rangle}{dt} = \langle \tau_{i-1}(1-\tau_i)\rangle - \langle \tau_i(1-\tau_{i+1})\rangle + \omega_A\langle 1-\tau_i\rangle - \omega_D\langle \tau_i\rangle, \tag{6}$$

where $\langle \cdots \rangle$ denotes the statistical average. At the boundaries, the densities evolve as

$$\frac{d\langle \tau_1 \rangle}{dt} = -\langle \tau_1(1-\tau_2)\rangle + \alpha\langle 1-\tau_1\rangle - \omega_D\langle \tau_1\rangle, \tag{7}$$

$$\frac{d\langle \tau_N \rangle}{dt} = \langle \tau_{N-1}(1-\tau_N)\rangle + \omega_A\langle 1-\tau_N\rangle - \beta\langle \tau_N\rangle. \tag{8}$$

First consider the steady state on a periodic system [where site $N+1$ is identified with site 1 and Eqs. (4) and (5) do not apply]. Assuming translational invariance, Eq. (6) is satisfied by $\langle \tau_i \rangle = \rho_{\rm eq}$, where

$$\rho_{\rm eq} = \omega_A/(\omega_A+\omega_D). \tag{9}$$

We refer to density (9) as the equilibrium density as it is the density obtained in the Langmuir absorption model [20]. Furthermore, it can be verified that the steady state of the system is given by a product measure with density of particles $\rho_{\rm eq}$.

We can apply particle-hole symmetry in order to simplify the discussion of the model. In the case of open boundary conditions, the system of equations (6)–(8) is invariant under the simultaneous exchanges $\alpha \leftrightarrow \beta$, $\omega_A \leftrightarrow \omega_D$, $i \leftrightarrow L-i$, and $\rho_i \leftrightarrow 1-\rho_i$.

III. MEAN-FIELD EQUATIONS AND CHARACTERISTICS

In the large N limit, we can make the continuum mean-field approximation to Eq. (6). First, we factorize correlation functions by replacing $\langle \tau_i(1-\tau_{i+1})\rangle$ with $\langle \tau_{i-1}\rangle(1-\langle \tau_i\rangle)$ [21], then we set

$$\langle \tau_{i\pm1}\rangle = \rho(x) \pm \frac{1}{N}\frac{\partial \rho}{\partial x} + \frac{1}{2N^2}\frac{\partial^2 \rho}{\partial x^2} \cdots . \tag{10}$$

Keeping leading order terms in $1/N$, one obtains

$$\frac{\partial \rho}{\partial \tau} = -(1-2\rho)\frac{\partial \rho}{\partial x} + \omega_D N[K-(1+K)\rho], \tag{11}$$

where $\tau = t/N$ and

$$K = \omega_A/\omega_D. \tag{12}$$

For the open system, we shall be interested in the scaling limit where

$$\Omega_A = \omega_A N \quad \text{and} \quad \Omega_D = \omega_D N \tag{13}$$

are finite as $N\to\infty$. The boundary conditions become $\rho(x=0)=\alpha$ and $\rho(x=1)=(1-\beta)$.

To understand the first-order differential equation (11), one can study the characteristics [22], which are defined for a quasilinear equation

$$a(x,\tau,\rho)\frac{\partial \rho}{\partial \tau} + b(x,\tau,\rho)\frac{\partial \rho}{\partial x} = c(x,\tau,\rho), \tag{14}$$

by the equations

$$\frac{dx}{d\tau} = \frac{b(x,\tau,\rho)}{a(x,\tau,\rho)}, \quad \frac{d\rho}{d\tau} = \frac{c(x,\tau,\rho)}{a(x,\tau,\rho)}. \tag{15}$$

Roughly speaking, characteristics are curves along which information about the solution propagates from the boundary conditions of the partial differential equation. Based on characteristics, Lighthill and Whitham [23] developed the theory of kinematic waves for equations with mass conservation

and showed how kinematic shock waves arise. Here, we generalize this picture to Eq. (11), where the number of particles is not conserved.

In the present case, the characteristics are given by

$$\frac{\partial x}{\partial \tau} = 1 - 2\rho, \tag{16}$$

$$\frac{\partial \rho}{\partial \tau} = \Omega_D[K - (1+K)\rho]. \tag{17}$$

Equations (16) and (17) are to be interpreted as kinematic waves [23], which propagate changes in the density, moving with speed $1-2\rho$ but with the density of the wave ρ itself changing with time. In the absence of creation and annihilation of particles, the density of the wave is constant in time and the waves propagate in straight lines. However, in the presence of creation and annihilation of particles, the waves will follow a curve in the x-t plane. For example, consider a density fluctuation starting at the left boundary with $\rho(0) = \alpha < 1/2$ and $\alpha < K/(1+K)$. Initially, the fluctuation will propagate to the right with speed $1-2\rho$ with its density increasing and speed decreasing. If $K/(1+K) < 1/2$, i.e., $K < 1$ the density will approach $\rho = K/(1+K)$ and the fluctuation will propagate to the right with a fixed speed. However, if $K/(1+K) > 1/2$, after some time the density of the fluctuation will reach $\rho = 1/2$ and the fluctuation will cease to propagate. Similarly, a kinematic wave starting at the right boundary with $\rho(1) = 1-\beta$, where $\beta < 1/2$ and $\beta < 1/(1+K)$ will travel to the left with decreasing density and decreasing speed.

When two characteristic lines cross, multivalued densities are implied; therefore, description (11) by a first-order differential equation breaks down. However, Lighthill and Whitham showed that the effect is that a shock, i.e., a discontinuity between the densities ρ_1 and ρ_2, arises at the meeting points of the two characteristics and this discontinuity travels with speed v_s. This speed is determined by balance of mass current to be [23]

$$v_s = \frac{\rho_2(1-\rho_2) - \rho_1(1-\rho_1)}{\rho_2 - \rho_1} = 1 - \rho_1 - \rho_2. \tag{18}$$

In the present case, although the mass is not conserved, the mass current through the shock still implies that its velocity is given by Eq. (18). Thus, for $\alpha < 1/2$, $\beta < 1/2$, we have the possibility of a shock forming then being driven to a position where the mass current through it is zero and the shock remains stationary. In the following section, we shall show how this picture is borne out by solving the steady-state mean-field equation.

IV. STEADY-STATE SOLUTION

Setting the time derivative of Eq. (11) to zero yields

$$(1-2\rho)\frac{\partial \rho}{\partial x} - \Omega_D[K - (1+K)\rho] = 0. \tag{19}$$

This is a first-order ordinary differential equation, which, in principle, can be solved analytically. The only difficulty is the occurrence of shocks in the solution. To construct the solution, we integrate from the left boundary $[\rho(0) = \alpha]$ to find a profile $\rho_l(x)$:

$$x = \frac{1}{\Omega_D}\int_{\alpha}^{\rho_l(x)} d\rho \frac{1-2\rho}{K-(1+K)\rho} \tag{20}$$

$$= \frac{1}{\Omega_D(1+K)}\left[2(\rho_l - \alpha) + \frac{K-1}{(1+K)}\ln\left|\frac{K-(1+K)\rho_l}{K-(1+K)\alpha}\right|\right], \tag{21}$$

and integrate from the right boundary $[\rho(1) = 1-\beta]$ to find a profile $\rho_r(x)$ through

$$1 - x = \frac{1}{\Omega_D(1+K)}\left[2(1-\beta-\rho_r) + \frac{K-1}{(1+K)}\ln\left|\frac{K-(1+K)(1-\beta)}{K-(1+K)\rho_r}\right|\right]. \tag{22}$$

To determine the full profile across the system, we have to match these two profiles at a shock whose position is to be determined.

A. The case $K=1$

First, we consider the special case of $K=1$, i.e., where the attachment and detachment processes have equal rates. The steady-state mean-field (MF) equation (19) reads

$$(2\rho - 1)\left(\frac{\partial \rho}{\partial x} - \Omega\right) = 0, \tag{23}$$

where $\Omega \equiv \Omega_A = \Omega_D$. This can be solved explicitly by a piecewise linear trial function leading to the condition: either $\rho(x) = \text{const} = \rho_{\text{eq}} = \frac{1}{2}$ or $\rho(x)$ has slope Ω. Note that this solution implies that higher derivatives in Eq. (10) vanish exactly.

First, we consider the parameter regime $\alpha < 1/2$, $\beta < 1/2$, where shock formation is possible. In order for the shock's position to be stable, i.e., for it not to be driven out of the system the shock's speed, as determined by Eq. (18), should be zero. Thus, the densities at the discontinuity should be related by $\rho_r(x_s) = 1 - \rho_l(x_s)$ and this determines the position of the shock x_s,

$$x_s = \frac{\beta - \alpha}{2\Omega} + \frac{1}{2}. \tag{24}$$

The height of the shock Δ is given by

$$\Delta = \rho_r(x_s) - \rho_l(x_s) = 1 - (\alpha + \beta) - \Omega \equiv \Omega_c - \Omega. \tag{25}$$

The last equation can be used in order to discuss the parameter dependence of the model. If Δ is positive and $0 < x_s < 1$, we find indeed a shock, which connects two domains with linear density dependence, as illustrated in Fig. 1. For

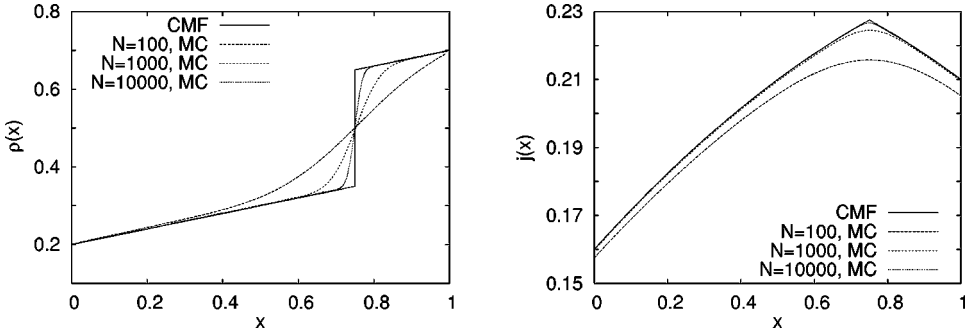

FIG. 1. Density $\langle \tau_i \rangle$ (left) and flow $\langle j_i \rangle = \langle \tau_i(1-\tau_{i+1}) \rangle$ (right) profiles for $\alpha=0.2$, $\beta=0.3$, $K=1$, and $\Omega=0.1$. For the MC results, we set $x=i/N$. The continuum mean-field theory results are compared to MC simulations of different system sizes. The agreement between MF and MC results is improved for larger system sizes.

$\Omega > \Omega_c$, one does not observe shock formation, but a section $(1-2\alpha)/2\Omega < x < 1-(1-2\beta)/2\Omega$, where $\rho = \frac{1}{2}$ (see Fig. 2).

In the ASEP, the line $\alpha=\beta$ is a phase boundary where shocks, between a high-density region coexisting with a low-density region, exist: Mean-field theory predicts the shock is at $x=1/2$ although the exact solution shows that the shock is actually delocalized and yields a linear density profile [7]. In the present case, although the shock's position is $x=1/2$ when $\alpha=\beta$, the role of this line changes and one does not observe a phase transition in crossing it.

Moreover, linear density profiles, which are observed for $\alpha+\beta+\Omega=1$, do not signify phase coexistence as for the ASEP, but indicate a vanishing height of the shock ($\Delta=0$). Also note that a strictly linear profile is observed only in the limit $N\to\infty$ in contrast to the disorder line of the ASEP (which is recovered in case of $\Omega=0$) where the constant density solution is valid for finite systems as well.

Next we discuss the case $\alpha>1/2$ and $\beta<1/2$. In this parameter regime, the density profile is given by

$$\rho(x) = \max\left[1-\beta-\Omega(1-x), \frac{1}{2}\right] \quad \text{for } x>0. \tag{26}$$

Equation (26) implies a singularity at $x=0$ since the boundary condition is $\rho(0)=\alpha$. For finite systems, the singularity at $x=0$ is softened as shown in Fig. 3. The behavior for $\alpha>1/2$ and $\beta<1/2$ can be obtained from particle-hole symmetry.

Finally, in the maximal current regime, the density profile in the limit $L\to\infty$ is given by

$$\rho(x) = \begin{cases} \alpha & \text{for } x=0 \\ 1/2 & \text{for } 0<x<1 \\ 1-\beta & \text{for } x=1. \end{cases} \tag{27}$$

i.e., apart from the two singular points $x=0$ and $x=1$, the density is constant.

The above results lead to the phase diagram shown in Fig. 4. Three phases can be distinguished, where the density profile does not reach the equilibrium $\rho_{\rm eq}$: The high- and low-density phase, where only a single domain exists in the system, the shock (see Fig. 1 for the corresponding density profile) region, where high- and low-density domain coexist. Then there are four phases, where the density profile has a section of constant density: The maximal-current phase (M) is obtained for $\alpha>1/2$ and $\beta>1/2$. If $\alpha>1/2$ and $1/2>\beta>1/2-\Omega$, we observe coexistence between a section of density 1/2 at the left and a linear profile as shown in Fig. 3. This phase is indicated by HM in the phase diagram, the corresponding low-density phase by LM. Finally, a section of constant density may coexist with a high- and low-density section (LMH) (see Fig. 2). We observe all phases only if $\Omega<1/2$. For $1/2<\Omega<1$, the high- and low-density phases vanish, while for $\Omega>1$ the formation of a shock is excluded. Our MC analysis illustrates the validity of the mean-field results for large system. This is in contrast to the case $\Omega=0$, where, e.g., for $\alpha=\beta$ the exact density profile even in the limit $N\to\infty$ is different from the mean-field results.

B. The case $K\neq 1$

In the case $K\neq 1$, the equilibrium density is different from $\rho=1/2$. Therefore, it is impossible to observe a maximal current phase because the bulk particle reservoirs destroy any maximal-current domain. The absence of the maximal-current phase originates in Eqs. (16) and (17): For the kinematic wave to be stationary one requires both Eqs. (16) and (17) to be zero, i.e., a bulk density satisfying both $\rho=1/2$ and $\rho=K/(K+1)$. It is also important to notice that the solution of the mean-field equations is not piecewise linear, i.e., higher order terms of Eq. (10) do not vanish. We

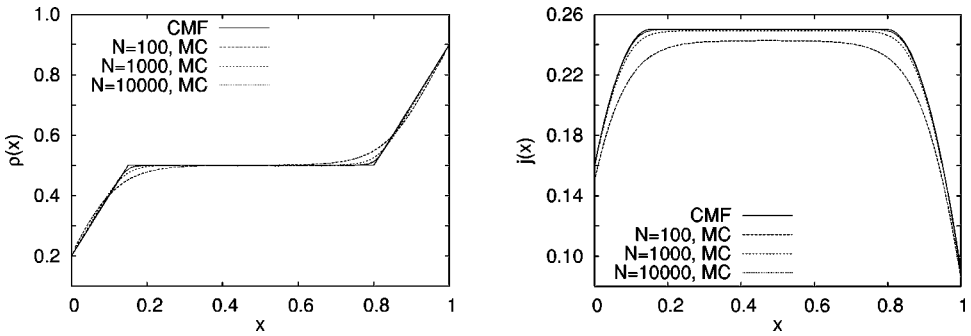

FIG. 2. Same as Fig. 1, but the parameters $\alpha=0.2$, $\beta=0.1$, $K=1$, and $\Omega=2.0$ are used. For this larger value of $\Omega=2.0$ shock formation is preempted by reaching the density $\rho_{\rm eq}=1/2$, see Eq. (9).

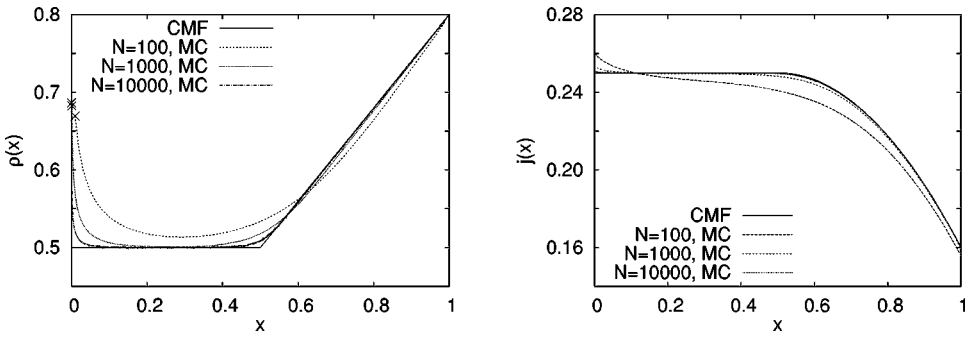

FIG. 3. Same as Fig. 1, but the parameters $\alpha=0.8$, $\beta=0.2$, $K=1$, and $\Omega=0.6$ are used. The average densities at the first site are indicated by symbols.

now analyze the mean-field equations for $K>1$ in more detail. The corresponding results for $K<1$ can be obtained from particle-hole symmetry. We consider separately the regime where $\alpha<1/2$ and $\beta<1/2$ and the complementary regime.

Case $\alpha<1/2$ *and* $\beta<1/2$. For low values of α and β, we expect the existence of a high- and low-density phase as well as the formation of shocks within a certain density regime as for the special case $K=1$. The transition lines can be obtained by analyzing the shock position, which is determined from the condition $\rho_r=1-\rho_l$. The shock separates a region where the density is given by Eq. (21) and a region where the density is given by Eq. (22).

For low α solution (21) may propagate all the way to the right boundary. If the density at the right boundary satisfies $\rho_l(1)<\rho_r(1)=\beta$ any shock will be driven out and the system will be dominated by ρ_l. This will be referred to as a low-density region (LD). The transition line between LD and S regions is given by the condition $\rho_l(1)=\beta$:

$$\Omega_D(1+K)=\left[2(\beta-\alpha)+\frac{K-1}{(1+K)}\ln\left|\frac{K-(1+K)\beta}{K-(1+K)\alpha}\right|\right]. \tag{28}$$

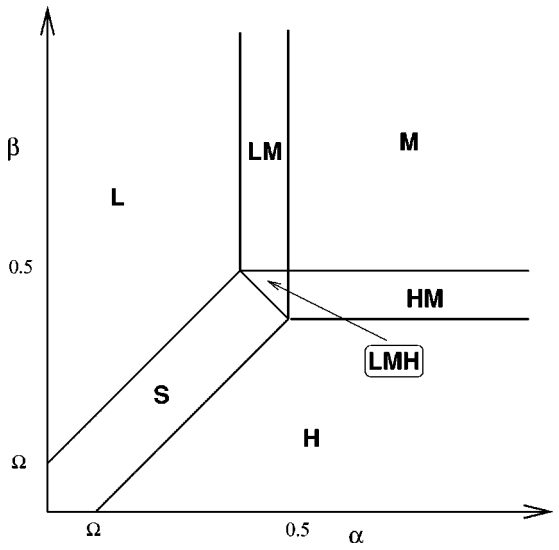

FIG. 4. Phase diagram for $K=1$ and $\Omega<1/2$. Indicated are the high- (H) and low-density (L) phase, the shock phase (S), the maximal current phase (M), and coexistence between a maximal current and low- (LM) or high-density (HM) domain. The LMH phase indicates the presence of three domains. A linear density profile is observed at the transition line between the LMH and S phase.

Similarly, for large β the solution ρ_r may propagate all the way to the left boundary where its density is $\rho_r(0)$. A shock between ρ_r and ρ_l will be driven to the left-hand boundary if $\rho_r(0)>1-\rho_l(0)=1-\alpha$. This will be referred to as the high-density region (HD). The transition line between HD and S regions is given by the condition $\rho_r(0)=1-\alpha$:

$$\Omega_D(1+K)=\left[2(\alpha-\beta)+\frac{K-1}{(1+K)}\ln\left|\frac{K-(1+K)(1-\beta)}{K-(1+K)(1-\alpha)}\right|\right]. \tag{29}$$

Cases $\alpha>1/2$ *or* $\beta>1/2$. For $\alpha>1/2$ or $\beta>1/2$ second-order terms (e.g., terms involving $\partial^2\rho/\partial x^2$) have to be retained in Eq. (11) for steady-state solutions to exist. However, the effect is, for example, in the case $\alpha<1/2$, $\beta>1/2$ at the right-hand boundary, that over a finite distance (of the order of $1/N$ in terms of the variable x) the second-order terms will match the density with that implied by ρ_r. Thus, the effect is that there is no shock and $\beta>1/2$ may for the purposes of the phase diagram may be *effectively* considered as $\beta=1/2$. In Fig. 5 comparison of direct simulations of the model when $\beta>1/2$ with density profiles obtained from the continuum theory (with β effectively considered as 1/2) indicate the validity of our approach in the large N limit.

For finite N, finite-size effects can partially be included by considering second-order terms in the mean-field description. Deviations between second-order mean-field and the exact results are due to the fluctuations of the shock, which are not correctly described by mean-field theory and have to be

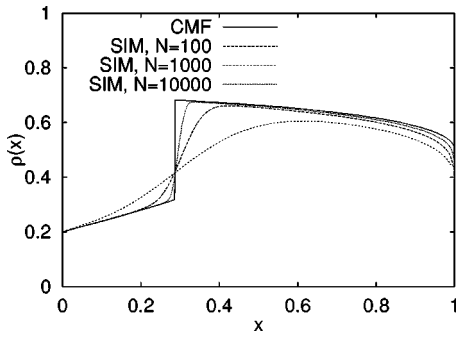

FIG. 5. Density profiles obtained from Monte Carlo simulations of the model for $\alpha=0.2$, $\beta=0.6$, $K=3$, $\Omega_D=0.1$, and $N=100$, 1000, 10 000. The full line gives density profiles obtained from the continuum mean-field theory, Eqs. (21) and (22) with β set equal to 1/2.

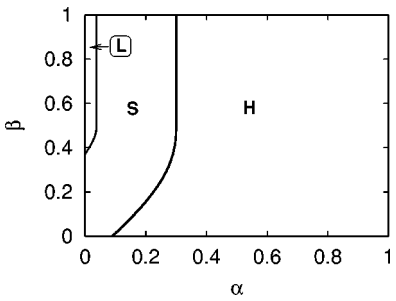

FIG. 6. Mean-field phase diagram for $\Omega_D=0.1$, $K=3$. (right). The phase boundaries between the low density (L), shock (S), and high density (H) phases are calculated by using Eqs. (28) and (29). Our results are in excellent agreement with the findings of Ref. [14] who analyzed numerically the second-order mean-field equations.

treated separately. This will be done in the following section. However, at this stage we note that the shock is indeed localized and that the width of the shock growth subextensively, i.e., the shock is sharp in the limit $N\to\infty$.

Phase diagram. Our analysis for $K\neq 1$ leads to the phase diagram shown in Fig. 6. We distinguish only three phases, i.e., the high- and low-density phase as well as the formation of shocks in an intermediate parameter regime. Compared to the case $K=1$, the number of phases is considerably reduced, due to the absence of a maximal-current phase as discussed above.

As the shock is sharp the fluctuations of the shock, which we treat in the following section, do not affect the phase boundaries. Therefore, we expect that the true phase diagram of the model is represented by Fig. 6.

V. DYNAMICS OF THE SHOCK

A qualitative understanding of the shock dynamics can be easily obtained from mass conservation, i.e., by means of the continuity equation. Compared to the ASEP additional source and sink terms have to be introduced, reflecting the on-site input and output of particles. This has been done in a recent work by Popkov *et al.* [24], who generalized the domain wall picture to models with particle input and output, where the continuity equation is given by

$$\frac{\partial\rho(x,t)}{\partial t}+\frac{\partial}{\partial x}j(\rho)=\Omega_A[1-\rho(x,t)]-\Omega_D\rho(x,t). \quad (30)$$

By inserting the known relation $j(\rho)=\rho(1-\rho)$ they recovered Eq. (11). The importance of the analysis by means of the hydrodynamic equation is given by the fact that this approach can be used for general models if the flow-density relation is known [24].

A step beyond the mean-field level is provided by interpreting the shock as a random walker. For the ASEP, on the line $\alpha=\beta$ the shock dynamics can be modeled as an unbiased random walk [25] and this allows one to calculate its diffusion constant. Moreover, one can generally consider kinematic shock wave dynamics as a biased random walker [26,27]. In the present case, we model the shock by a random walker with the site-dependent hopping rates

$$w_l(i)=\frac{j_-(x)}{\Delta(i)}, \quad w_r(i)=\frac{j_+(x)}{\Delta(i)}, \quad (31)$$

where w_l (w_r) denotes the hopping rate to the left (right), $j_-(i)$ [$j_+(i)$] the flux in the low- (high-) density domain at site i, and $\Delta(i)$ the height of the shock at position i. Modeling the shock dynamics as a random walk with reflecting boundary conditions allows us to derive analytical expressions for the stationary distribution $p_s(i)$ of shock positions. The stationary distribution $p_s(i)$ has to fulfill the condition

$$w_r(i)p_s(i)=w_l(i+1)p_s(i+1). \quad (32)$$

One can solve this discrete equation explicitly, but it is simplest to proceed by making a continuum approximation. We expand the probability distribution to first order in $1/N$, as in Eq. (10), and use the stationarity condition to obtain the differential equation

$$y'(x)+Ny(x)\left(1-\frac{w_r(x)}{w_l(x)}\right)=0, \quad (33)$$

where $y(x)=p(x)w_l(x)$. The solution of this equation is given by

$$p(x)=\frac{\tilde{p}(x)}{\mathcal{N}}=\frac{1}{\mathcal{N}w_l(x')}\exp\left[-N\int_{x_0}^{x}\left(1-\frac{w_r(x')}{w_l(x')}\right)dx'\right], \quad (34)$$

where $\mathcal{N}=\int_0^1\tilde{p}(x)dx$. Explicit expressions of the distribution can be given in case of $K=1$, which will be discussed in detail. For this case, we get the unnormalized distribution

$$\tilde{p}(x)=\left(x+\frac{\alpha}{\Omega}\right)^{[N(1-\Delta)\Delta]/\Omega-1}\left(\frac{1-\alpha}{\Omega}-x\right)^{[N(1+\Delta)\Delta]/\Omega-1}$$
$$\sim e^{-C(x-x_s)^2}, \quad (35)$$

where $C=4N\Omega\Delta/[(1-\Delta)(1+\Delta)]$. The Gaussian is obtained from a logarithmic expansion of the exponent, which is justified in the limit $N\to\infty$ [29].

Using the random walk picture, the density profile can be obtained from the shock distribution $p(x)$ through [27]

$$\rho(x)=\rho_r(x)\int_0^x p(x')dx'+\rho_l(x)\int_x^1 p(x')dx'. \quad (36)$$

The Gaussian approximation of $p(x)$ leads to the following form of the density profile:

$$\rho(x)=\frac{\Delta}{2}\left[1+\mathrm{erf}\left(2\sqrt{\frac{N\Omega\Delta}{(1+\Delta)(1-\Delta)}}(x-x_s)\right)\right]+\Omega x+\alpha. \quad (37)$$

In order to check the validity of this simple phenomenological picture, we compare the analytic predictions (37) for different density profiles in the S phase with results of MC simulations [30]. Figure 7 shows that the random walk pre-

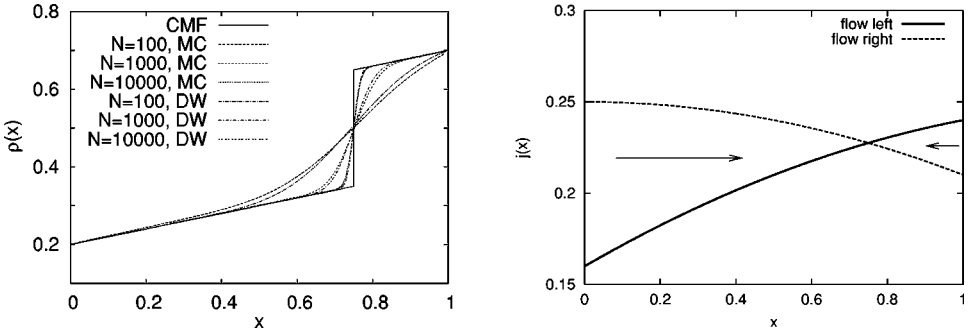

FIG. 7. Left: Density profiles in comparison with the DW predictions. The chosen parameters are $\alpha=0.2$, $\beta=0.3$, $\Omega=0.2$, and $K=1$. Right: Flow profile of the left (solid line) and right domain (dashed line) for same set of parameters. The arrows indicate the bias of the random walker.

dictions are in good agreement with the MC results and the accuracy of the random walk description improves for larger system sizes.

From Eq. (37) it follows that the width of the shock scales as $N^{-\nu}$ with $\nu=1/2$ as was found numerically in Ref. [14].

VI. CONCLUSION

The model studied by Parmeggiani, Franosch, and Frey [14] can be interpreted as a generic model for the collective behavior of molecular motors. The physics of the model is governed by the competition of different particle reservoirs and the stationary flow of the self-driven particles. In the case of periodic boundary conditions, one easily verifies that the stationary state of the process is described by a product measure. More interesting features are observed in the case of open boundary conditions. Here, when the rates for attachment and deletion of particles in the bulk are appropriately scaled with system size, localization of a shock arises between the region of the system controlled by the left boundary and the region controlled by the right boundary.

Most of the features of this model can be explained by a mean-field analysis, which we believe to be correct in the limit of large system size. This is supported by Figs. 1, 2, 3, and 5, where direct simulations for the density profiles converge for large system sizes to our mean-field predictions. In view of this, we believe the mean-field phase diagrams, Figs. 4 and 6, are in fact exact.

By considering the characteristics of the mean-field equations, the formation and localization of the shock can be explained: The characteristic solutions propagating from the left and right boundaries are matched at the shock whose position is fixed by the condition that the mass current through the shock is zero. In the presence of a shock, the leading finite-size corrections are due to the fluctuations of the shock position, which can be described by mapping the dynamics of the shock to a random walk with site-dependent hopping rates.

Apart from the importance of the ASEP with creation and annihilation of particles in the bulk as a generic model for molecular motors it is of special interest for the general formalism of nonequilibrium statistical mechanics. In particular, one can interpret the bulk nonconservation of particles as exchange of particles with a bulk reservoir [28]. In this way, the model can be thought of as a grand-canonical counterpart to the ASEP. As the ASEP and its variants can be analyzed in detail, they might help us to understand aspects of different ensembles in the context of nonequilibrium statistical mechanics.

ACKNOWLEDGMENTS

R.J. and L.S. acknowledge support from the Deutsche Forschungsgemeinschaft under Grant No. SA864/2-1. M.R.E. thanks Universität des Saarlandes for kind hospitality during a visit supported by DFG (SFB277).

[1] T. Liggett, *Interacting Particle Systems: Contact, Voter and Exclusion Processes* (Springer-Verlag, Berlin, 1999).
[2] G. M. Schütz, in *Phase Transitions and Critical Phenomena*, Vol. 19, edited by C. Domb and J. L. Lebowitz (Academic Press, San Diego, 2001).
[3] *Nonequilibrium Statistical Mechanics in One Dimension*, edited by V. Privman (Cambridge University Press, Cambridge, 1997).
[4] D. Chowdury, L. Santen, and A. Schadschneider, Phys. Rep. **329**, 199 (2000).
[5] H. Hinrichsen, Adv. Phys. **49**, 815 (2000).
[6] A. Schadschneider, Eur. Phys. J. B **10**, 573 (1999).
[7] B. Derrida, M. R. Evans, V. Hakim, and V. Pasquier, J. Phys. A **26**, 1493 (1993).
[8] G. Schütz and E. Domany, J. Stat. Phys. **72**, 277 (1993).
[9] M. R. Evans, N. Rajewsky, and E. R. Speer, J. Stat. Phys. **95**, 45 (1999).
[10] J. de Gier and B. Nienhuis, Phys. Rev. E **59**, 4899 (1999).
[11] N. Rajewsky, L. Santen, A. Schadschneider, and M. Schreckenberg, J. Stat. Phys. **92**, 151 (1998).
[12] B. Derrida, J. L. Lebowitz, and E. R. Speer, Phys. Rev. Lett. **89**, 030601 (2002).
[13] For a review, see S. A. Janowsky and J. L. Lebowitz Nonequilibrium Statistical Mechanics in One Dimension (Ref. [3]), Chap. 13, and references therein.
[14] A. Parmeggiani, T. Franosch, and E. Frey, Phys. Rev. Lett. **90**, 086601 (2003).
[15] B. Alberts, D. Bray, and J. Lewis, *Molecular Biology of the Cell* (Garland, New York, 1994).
[16] J. Howard, *Mechanics of Motor Proteins and the Cytoskeleton* (Sinauer, Sunderland, 2001).

[17] *Physics of Bio-Molecules and Cells*, edited by H. Flyvbjerg, F. Jülicher, P. Ormos, and F. David (Springer, Heidelberg, 2002).
[18] J. Howard, Nature (London) **389**, 561 (1997).
[19] F. Jülicher, A. Ajdari, and J. Prost, Rev. Mod. Phys. **69**, 1269 (1997).
[20] H. T. Davis *Statistical Mechanics of Phases, Interfaces and Thin Films* (Wiley-VCH, New York, 1996).
[21] B. Derrida, E. Domany, and D. Mukamel, J. Stat. Phys. **69**, 667 (1992).
[22] L. Debnath, *Nonlinear Partial Differential Equations for Scientists and Engineers* (Birkhäuser, Boston, 1997).
[23] M. J. Lighthill and G. B. Whitham, Proc. R. Soc. London, Ser. A **229**, 281 (1955).
[24] V. Popkov, A. Rákos, R. D. Willmann, A. B. Kolomeisky, and G. M. Schütz, Phys. Rev. E (to be published), e-print cond-mat/0302208.
[25] B. Derrida, M. R. Evans, and K. Mallick, J. Stat. Phys. **79**, 833 (1995).
[26] A. Kolomeisky, G. M. Schütz, E. B. Kolomeisky, and J. P. Straley, J. Phys. A **31**, 6911 (1998).
[27] L. Santen and C. Appert, J. Stat. Phys. **106**, 187 (2002).
[28] R. Lipowsky, S. Klumpp, and T. M. Nieuwenhuizen, Phys. Rev. Lett. **87**, 108101 (2001); S. Klumpp and R. Lipowsky, e-print cond-mat/0304681.
[29] We also checked the accuracy of the Gaussian approximation by comparing with the numerically determined exact distribution $p(x)$. The resulting density profiles are numerically indistinguishable for the system sizes shown in Fig. 7.
[30] In order to pass the transient regime, we performed initially $10^5 L$ local updates. Measurements of the density profiles have been averaged over 10^8 sweeps. The statistical error of the MC data is of the order of the line width.